Imogolite: an aluminosilicate nanotube endowed with low cytotoxicity and genotoxicity

Bianca Maria Rotoli[†], Patrizia Guidi[§], Barbara Bonelli[⊥], Margherita Bernardeschi[§], Massimiliano G. Bianchi[¶], Serena Esposito[‡], Giada Frenzilli[§], Paolo Lucchesi[§], Marco Nigro[§], Vittoria Scarcelli[§], Maura Tomatis[^], Pier Paolo Zanello[†], Bice Fubini[^*], Ovidio Bussolati[†*] Enrico Bergamaschi[¶]

Dept. of Biomedical, Biotechnological and Translational Sciences (SBiBiT)[†] and Dept. of Clinical and Experimental Medicine[¶], University of Parma, 43125 Parma, Italy

Dept. of Clinical and Experimental Medicine, University of Pisa, 56126 Pisa, Italy[§]

Dept. of Applied Science and Technology and INSTM, Unit of Torino Politecnico, Politecnico di Torino, 10129 Turin, Italy[⊥]

Dept. of Civil and Mechanical Engineering, University of Cassino and Southern Lazio, 03043 Cassino, Italy[‡]

Dept. of Chemistry, and "G. Scansetti" Interdepartmental Center for Studies on Asbestos and other Toxic Particulates, University of Torino, 10125 Turin, Italy[^]

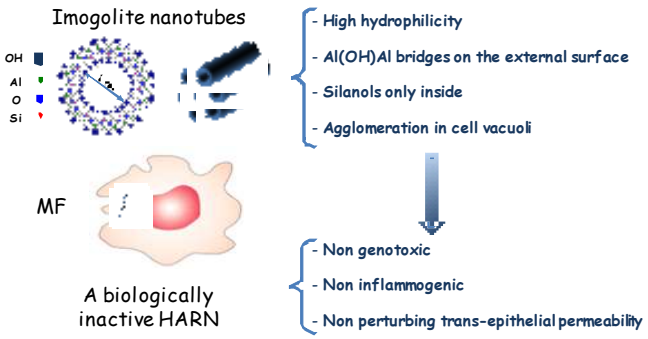
Imogolite nanotubes
OH
Al
O
Si
- High hydrophilicity
- Al(OH)Al bridges on the external surface
- Silanols only inside
- Agglomeration in cell vacuoli
MF
A biologically inactive HARN
- Non genotoxic
- Non inflammogenic
- Non perturbing trans-epithelial permeability

ABSTRACT

High-Aspect Ratio Nanomaterials (HARN) - typically single-walled (SWCNT) or multi-walled carbon nanotubes (MWCNT) - impair airway barrier function and are toxic to macrophages. Here we assess the biological effects of nanotubes of imogolite (INT), a hydrated alumino-silicate [$(OH)_3Al_2O_3SiOH$] occurring as single-walled NT, on murine macrophages and human airway epithelial cells. Cell viability was assessed with resazurin. RT-PCR was used to study the expression of *Nos2* and *Arg1*, markers of classical or alternative macrophage activation, respectively, and nitrite concentration in the medium was determined to assess NO production. Epithelial barrier integrity was evaluated from the Trans-Epithelial Electrical Resistance (TEER). Potential genotoxicity of INT was assessed with Comet and Cytokinesis-block Micronucleus Cytome assays. Compared to MWCNT and SWCNT, INT caused much smaller effects on RAW264.7 and MH-S macrophage viability. The incubation of macrophages with INT at doses as high as 120 μg/cm^2 for 72h did not alter either *Nos2* or *Arg1* expression nor increased NO production, while IL6 was induced in RAW264.7 but not in MH-S cells. INT did not show any genotoxic effect in RAW264.7 and A549 except for the decrease of DNA integrity observed in epithelial A549 cells after the treatment with the highest dose (80 μg/cm^2). No significant change in permeability was recorded in Calu-3 epithelial cells monolayers exposed to INT, while comparable doses of both SWCNT and MWCNT lowered TEER. Thus, in spite of their fibrous nature, INT appear not markedly toxic for *in vitro* models of lung-blood barrier cells.

Key Words: imogolite, genotoxicity, cytotoxicity, macrophages, airway epithelium, trans-epithelial electrical resistance, nanotubes

INTRODUCTION

Different kinds of nanomaterials are increasingly produced for several technical and bio-medical applications, because of their peculiar mechanical and electrical properties. However, the consequences of the interaction of these novel materials with biological systems are often not completely understood and their potentially toxic effects are still the object of debate and cause of concern.[1-4]

Among nanomaterials, carbon nanotubes (CNT) and other High Aspect Ratio Nanomaterials (HARN), are a cause for concern due to their asbestos-like morphology. Evidence exists that a fraction of CNT reaches the pleura, with consequent retention of long fibres, inflammation, fibrosis and several pathologies, including mesothelioma, similar to that observed for asbestos fibres.[5] The question arises whether any nanotube with close morphology would exert the same effect or different materials might behave in quite different ways.[6,7]

Imogolite is a nanotubular aluminosilicate with stoichiometry $(OH)_3Al_2O_3SiOH$ that naturally occurs in volcanic soils and may be also obtained with high purity by sol-gel synthesis.[8,9] Imogolite nanotubes (INT) exhibit Al-O-Al and Al(OH)Al groups at the outer surface and SiOH groups at the inner surface, as shown in Scheme 1. Typically, INT have inner diameter of about 1.0 nm, outer diameter of 2.0-2.7 nm, and variable length in the micrometer range,[10] thus structurally resembling single-walled carbon nanotubes (SWCNT).

Once formed, INT are expected to arrange as a porous network of interwoven bundles with three kinds of pores, depicted in Scheme 2:[11] (A) intra-tube nanopores (about 1 nm wide); (B) inter-tube pores corresponding to the spacing among three aligned nanotubes in a regular packing (0.3-0.4 nm wide) and (C) slit mesopores among bundles.

Besides being a subject of interest in the pedological field, INT are endowed with properties[12-14] that render them candidates for several industrial applications, such as separation or storage of gas,[14-16] uptake of anions and cations from water[17,18] and catalysis.[9,19] This variety of potential

applications explain the interest in synthesizing imogolite-like structures, such as single-walled or double-walled aluminogermanate nanotubes.[20-24]

Very little information is available on INT toxicity. A study concerning an aluminogermanate imogolite analogue reports length and dose-dependent genotoxic effects, in the absence of significant cytotoxic events in cultured human fibroblasts.[25] However,it must be noted that, besides their different chemical composition, aluminogermanate NT are shorter in length and have a larger diameter, finally exhibiting a markedly different morphology with respect to proper INT. Since INT can be synthesized and aligned into densely-packed arrays oriented in a single dimension,[26] they may be of interest as a biological scaffold that mimics the fibrous morphology of type I collagen. A single study on possible biomedical applications of INT[26] shows indeed good bio-compatibility in osteoblast cultures, in terms of cell spreading, cell proliferation, and enhanced matrix mineralization; however, possible toxicity has not been investigated.

The present study has been undertaken to assess INT biological effects *in vitro*, using macrophages and airway epithelial cells, two cell models in which HARN toxicity has been repeatedly investigated. For this purpose, INT with controlled morphology have been synthesized and employed in several toxicity-related tests. Physico-chemical characterization has included material morphology, surface charge, specific surface area, and hydrophilicity. In order to assess a large number of properties usually associated with lung damage, the ability to generate free radical species in cell-free test, cellular uptake, cell viability, genotoxicity, macrophage activation, and changes in epithelial permeability have been investigated.

EXPERIMENTAL PROCEDURES

Materials

Imogolite nanotubes (INT) were synthesized according to the method described previously:[9,27] at 20°C TEOS (Tetra-ethoxysilane) and Al(s-butoxide)$_3$ were added to a 75 mM aqueous solution of $HClO_4$ in the molar ratios Si: Al: $HClO_4$ = 1 : 2 : 1. A slight excess of TEOS was used, in order to prevent preferential formation of aluminium hydroxide during hydrolysis. The solution was stirred for 18 h, diluted to 20 mM in Al, autoclaved at 100°C for 4 days, dialyzed for 4 days against de-ionized water and then dried at 50°C.

Commercial SWCNT (Aldrich 636797, Lot 12526AE, 1.1 nm x 5–15 μm, BET 400 m^2/g according to manufacturer) were also obtained from Sigma-Aldrich. They consist of SWCNT (> 50%) and of other nanotubes (MWCNT and double-walled CNT, 40%) with < 5% amorphous carbon and traces of metals (Co 0.6%, Mg 1.2%, Mo 0.1%)), as declared by the supplier. Commercial MWCNT (Aldrich 659258, 110-170 nm x 5-9 μm) were obtained from Sigma–Aldrich, Milan, Italy. MWCNT Aldrich 659258 have a SSA 22.6 ± 0.38 m^2/g and are largely made of multi-walled nanotubes (at least 90%), with residual amorphous carbon.

Characterization of imogolite nanotubes

Field Emission Scanning Microscopy (FESEM) pictures of the three nanomaterials were collected with a high resolution FESEM instrument (LEO 1525) equipped with a Gemini Field Emission Column.

Specific Surface Area (SSA) was measured according to the BET (Brunauer-Emmett-Teller) method. N_2 adsorption isotherms were measured at –196 °C on INT previously outgassed at 300 °C in order to remove water and other atmospheric contaminants, but still preserving INT integrity (Quantachrome Autosorb 1C instrument). NL-DFT (Non Local Density Functional Theory)[28] method was used to evaluate pore size distribution (PSD) by applying a N_2-silica kernel.

The surface electrical charge of INT was evaluated by measuring their ζ-potential both in water and in two complete cell culture media, namely F12 and MEM. ζ-potential curves as a function of pH were measured at 25°C by means of electrophoretic light scattering (ELS) technique (Zetasizer Nano- ZS, Malvern Instruments, Worcestershire, U.K.). INT suspensions were obtained after 2 min sonication with an ultrasonic probe (100 W, 20 kHz, Sonoplus; Bandelin, Berlin, Germany); the pH of the suspension was adjusted by adding either 0.1 M HCl or 0.1M NaOH.

Surface hydrophilicity was evaluated by gas-solid adsorption microcalorimetry. A heat flow microcalorimeter (Calvet-type, Setaram, France) connected to a high-vacuum gas-volumetric glass apparatus was employed. Subsequent doses of water vapor were admitted onto the sample and adsorbed amounts, released heat and equilibrium pressure were measured for each dose when the thermodynamic equilibrium was attained. The calorimeter was maintained at 30°C throughout the adsorption experiment. The equilibrium pressure (p H_2O, Torr) was monitored by means of a transducer gauge (Barocell 0–100 Torr, Edwards). A typical adsorption sequence comprised three subsequent runs, with the following procedure: (i) dosing successive amounts of water vapor onto the sample up to a defined equilibrium pressure, typically 10 Torr (Ads I), (ii) desorption at 30°C under vacuum, and (iii) readsorption of similar doses up to the same pressure, in order to evaluate the fraction of adsorbate which is reversibly held at the surface (Ads II). Adsorbed amounts were normalized to the unit surface area (n_{ads}, μmol/m^2) and plotted in the form of volumetric isotherms. Differential heats of adsorption, which represent the enthalpy changes ($q^{diff} = -\Delta_{ads}H$) associated with the process, were plotted as a function of the increasing water uptake. Prior to the adsorption measurement, the sample was outgassed in the calorimetric cell for 2 h at 150°C, and subsequently transferred into the calorimetric vessel without any exposure to the atmosphere.

Free radical generation in cell-free-test

Free radical release, upon incubation of INT with either H_2O_2 (yielding hydroxyl radicals) or sodium formate (yielding carbon centred radicals as a consequence of homolytic cleavage of a C-H bond), was measured by Electron Paramagnetic Resonance (EPR) spectroscopy using the Spin Trapping technique with 5,5'-dimethyl-1-pyrroline-*N*-oxide (DMPO) as trapping agent according to a technique well established in our laboratory.[29] Two amounts (7 and 70 mg) of powder were tested. $HO^{\bullet}$ generation was measured by suspending INT in 500 µl of 0.5 M phosphate buffer (pH = 7.4), then adding 250 µl of 0.17 M DMPO and 500 µl of 0.2 M H_2O_2. The production of $CO_2^{\bullet-}$ radicals was measured by suspending INT in 500 µl of 0.17 M DMPO, then adding 500 µl of a 2 M sodium formate solution in 0.5 M phosphate buffer. The number of radicals released is proportional to the intensity of the EPR signal measured by double integration. Kinetics of free radical yield was followed for at least 1 h.

Cell culture and treatments

For viability and gene expression studies two murine macrophage cell lines have been used: RAW264.7, obtained from the Istituto Zooprofilattico Sperimentale della Lombardia (Brescia, Italy) and MH-S,[30] obtained from prof. Dario Ghigo, Department of Biochemistry, University of Turin. Cells were cultured in RPMI. These lines, have been extensively used in toxicological studies.[31-35]

For genotoxicity studies, RAW264.7 cells, cultured in Minimal Essential Medium (MEM), and alveolar carcinoma A549 cells, cultured in F-12 medium, were provided by prof. Lucia Migliore, University of Pisa. RAW264.7 and A549 cells were selected as they are widely used to assess genotoxicity effects of nanomaterials in vitro.[36,37]

For studies of epithelial permeability, Calu-3 cells, derived from a human lung adenocarcinoma,[38] were obtained from the Istituto Zooprofilattico Sperimentale della Lombardia (Brescia, Italy) and

cultured in Eagle's Minimum Essential Medium (EMEM) supplemented with 1mM sodium pyruvate. Calu-3 cells have been extensively used in recent studies to investigate airway epithelium permeability.[39-45]

For all cell types, media were supplemented with 10% fetal bovine serum (FBS), 1% Pen/Strep and 2 mM glutamine and cultures were maintained at 37°C under a humidified atmosphere of 5% CO_2/95% air.

Before the experiments, INT, SWCNT and MWCNT were heated at 220 °C for 3h to eliminate possible contamination from lipopolysaccharide. For viability and gene expression experiments, after cooling at room temperature, nanomaterials were dispersed at a concentration of 1mg/ml in sterile phosphate-buffered saline (PBS) to obtain stock suspensions for a series of experiments. Immediately before each experiment, the materials were extensively vortexed, sonicated three times for 15 min in a Bransonic Ultrasound bath, and then added to normal growth medium to reach the desired concentration. No detergent was used to improve the solubility of nanomaterials in aqueous solutions. After the addition, CNT and INT tend to precipitate and to form more or less expanded agglomerates, clearly detectable with optical microscopy, that come into contact with the cell monolayer (not shown). For genotoxicity studies the highest dose was obtained dispersing the nanotubes in the medium and obtaining the other doses by dilution in the wells.

Nominal doses were expressed as μg of nanotubes per cm^2 of monolayer.

Viability

Cell viability of RAW264.7 and MH-S was tested with the resazurin method[46] in cells seeded in 96-well dishes (30 x 10^3 cells/well). According to this method, viable cells reduce the non-fluorescent compound resazurin into the fluorescent resorufin that accumulates into the medium. After the exposure to INT or CNT, carried on in thermostat, cells were incubated for 1 h with fresh, serum-

free medium supplemented with 44 μM resazurin; fluorescence was then measured at 572 nm with a fluorimeter (Wallac 1420 Victor2 Multilabel Counter, Perkin Elmer).

For Calu-3 monolayers grown in a double chamber culture system (see below), resazurin was added at both sides of the monolayer and fluorescence was measured in the apical compartment.[47]

The possible interference of the nanomaterials with resazurin was assessed both in the absence and in the presence of cells. While MWCNT and INT (both at the dose of 80 $\mu g/cm^2$ of culture surface) did not appreciably quench resorufin fluorescence, SWCNT produce a significant dose-dependent quenching (data not shown). Therefore, the data on vitality relative to treatment with SWCNT were adequately corrected, taking into account the contribution of quenching, through the empirical, experimentally derived formula $F_C = F_M \cdot (1 + 0.0083 \cdot D_S)$ where F_C is the corrected fluorescence, F_M is the measured fluorescence, D_S is the dose of SWCNT (expressed as $\mu g/cm^2$).

Gene expression

Total RNA, extracted from cells, seeded in 6-well dishes (300 x 10^3 cells/well) and grown to subconfluency, with RNeasy Mini Kit® (Qiagen S.p.a., Milano, Italy), was reverse transcribed and 40 ng of cDNA amplified and treated as described previously.[48] The forward and reverse primers (5 pmol each) used are detailed in Table I. Quantitative PCR was performed in a 36 well Rotor Gene™ 3000, version 5.0.60 (Corbett Research, Rotor-Gene™ 3000, version 5.0.60, Mortlake, Australia). Fluorescence was monitored at the end of each extension step. A no-template, no reverse transcriptase control was included in each experiment. At the end of the amplification cycles a melting curve analysis was added. RT-PCR data are expressed as the ratio between the mRNA of interest and that of *Gapdh*.

Nitric oxide production

The production of NO was assessed through the quantification of nitrites, stable derivatives of NO, in the culture medium, employing a fluorimetric approach described previously.[49]. Nitrite concentration was calculated from a calibration curve performed with $NaNO_2$ standards and expressed in nmoles/ml extracellular medium (μM). Calibration curves, performed in the absence or in the presence of INT at the dose of 120 $\mu g/cm^2$ of culture surface, were comparable (data not shown) indicating that INT do not interfere with the method.

Comet assay

RAW264.7 and A549 cells were seeded and treated for DNA damage evaluation as previously described.[50] The single-cell gel electrophoresis (or Comet assay) was performed according to Singh et al.[51] with slight modifications. Briefly, cell suspensions were embedded in agarose, spread onto microscope slides, lysed (NaCl 2.5 M, Na_2EDTA 100 mM, Trizma Base 10 mM, 10% dimethylsulphoxide, 1% Triton X-100; pH 10) and kept for at least 1 h at +4°C in the dark. Successively, slides were treated with alkali (NaOH 300 mM, Na_2EDTA 1 mM, pH >13) and electrophoresed for 20 min at 25 V and 300 mA. After run, slides were neutralized with Tris–HCl (0.4 M, pH 7.5), stained with ethidium bromide and observed under a fluorescence microscope (400×). The percentage of DNA migrated towards the anode (tail DNA) was quantified by an image analyser (Kinetic Imaging Ltd, Komet, Version 5). At least 25 nuclei per slide and two slides per sample were scored, and the average value was calculated. A total of 300 cells were scored for experimental point. Three independent experiments were carried out for each treatment. Cell viability was assessed by Trypan blue dye exclusion technique.

Cytokinesis-block Micronucleus Cytome assay

RAW264.7 and A549 cells were seeded and treated for cytogenetic studies as previously reported.[50] Cytochalasin B (4 μg/ml) was added 44 h after seeding. Cells were washed with Hanks' Balanced Salt Solution 72 h after seeding, detached and centrifuged at 500xg for 10 min. Pellets were treated with 1 ml of hypotonic solution (KCl 0.075 M) at 37°C, pre-fixed with methanol:acetic acid 3:5. Cells were centrifuged and pellets suspended in a fresh and cold (+4°C) fixative solution (methanol and acetic acid 7:1), then kept at +4°C for at least 30 min. After a second fixative step, cells were dropped onto slides and stained with 2% Giemsa. 1000 binucleated cells for slide were analyzed and 2 slides for each well were set up for a total of 4000 cells scored per treatment. Two samples were set up for a total of 4000 cells scored per treatment. Two independent experiments were carried out for each treatment. Micronuclei (MN) and nucleoplasmic bridges (NPB) were scored according to the criteria set by Fenech[52,53] and their frequency was recorded as ‰ of binucleated cells.

Trans-Epithelial Electrical Resistance

For measurements of the Trans-Epithelial Electrical Resistance (TEER), Calu-3 cells were seeded into double chamber culture inserts on membrane filters (pore size of 0.4 μm) for Falcon 24-well-multitrays (Cat. N° 3095, Becton, Dickinson & Company, Franklin Lakes, NJ, USA), at a density of 75×10^3 cells/300 μl. Measurements of TEER were made on monolayers grown for 10–14 d, using an epithelial voltohmeter (EVOM, World Precision Instruments Inc., Sarasota, FL, USA). Materials were added in the apical chamber from a 1 mg/ml stock solution without changing the medium. TEER changes were expressed as the percentage of the initial value adjusted for control cell layers according to the equation:[54]

$$\Delta_{TEER}\ \% = \frac{\text{Final TEER}_{treated}}{\text{Final TEER}_{control}} \times \frac{\text{Initial TEER}_{control}}{\text{Initial TEER}_{treated}} \times 100$$

Internalization

To test INT internalization, cells exposed for 24 h to 80 μg/cm^2 of INT were centrifuged, washed and treated with Karnovsky fixative for 5 h at 36.4°C, washed in 0.1 M sodium cacodylate solution overnight, post-fixed in 1% osmium tetroxide for 2h in the dark at room temperature, newly washed with the same buffer solution and dehydrated in graded series of ethanol. Samples were pre-embedded in Epon Araldite–propylene oxide 1:1 mixture overnight, followed by pure Epon Araldite for 6 h, then embedded in Epon Araldite at 60°C for 48 h.[55] Ultra-thin sections (70–90 nm) were cut using a Reichert-Jung Ultracut E ultramicrotome, collected on 200-mesh carbon-coated copper grids stained with uranyl acetate and lead citrate and observed with a JEOL 100 SX transmission electron microscope.

Statistical analysis

Values of viability, TEER, and nitrite production were analyzed with ANOVA using post hoc Bonferroni test and expression data were evaluated with a t-test for unpaired data.

Multifactor Analysis of Variance (MANOVA) was carried out on Comet and Cytome assay data, considering dose, experimental time, culture, cell type, and experiment as factors. The Multiple Range Test (MRT) was performed in order to detect differences among different experimental groups. Level of statistical significance was considered for p values < 0.05.

Reagents

L-glutamine, FBS, and culture media were purchased from EuroClone SpA, Pero, Milan, Italy. Recombinant human interleukin-4 (IL-4) was obtained from RELIAThech GmbH, Wolfenbuttel, Germany. Sigma–Aldrich (Milan, Italy) was the source of all the other chemicals.

RESULTS

Characterization of imogolite nanotubes

Figure 1, Panel a, shows a FE-SEM picture of imogolite nanotubes (INT). As reported in the literature and illustrated in Scheme 2, INT are several microns long and arranged into bundles forming an interwoven porous network so that it is not possible to observe "single" INT, but only bundles.[9,14] No other morphology, such as spherical particles attributable to the presence of proto-imogolite, a common impurity in INT obtained by synthesis,[9] was observed by FE-SEM analysis, indicating that a pure INT sample was obtained. A picture of SWCNT is reported in Figure 1, Panel b, confirming the presence of MWCNT besides actual SWCNT, as reported in the Materials and Methods section. Image of MWCNT shows the presence of large, 100–200 nm wide tubes (Panel c).

Figure 2a reports the N_2 isotherm measured at –196 °C on dehydrated INT; a type I isotherm was observed, with no hysteresis loop, as expected for INT.[9] The corresponding BET SSA was 384 $m^2 g^{-1}$ and the overall microporous area (due to intra-tube pores) was indeed 261 $m^2 g^{-1}$: Figure 2b reports the PSD as obtained by applying the NL-DFT method to isotherm adsorption branch: a major family of pores was seen with maximum diameter at about 1.0 nm, assigned to intra-tube pores; larger (inter-tubes) pores are also present, in agreement with literature reports.[9]

Measurements of the ζ potential of INT are reported in Figure 3. INT in water was positively charged at low pH and the point of zero charge (PZC) was at pH = 9.9, which is close to values reported in the literature for alumina particles.[56] This result is in agreement with the composition of INT external surface that exposes only Al-O-Al groups and Al(OH)Al bridges and should, therefore, behave as a hydrated aluminium oxide. According to the literature,[13] depending on pH the outer surface of INT may carry a positive net charge, whereas the inner surface would carry a corresponding negative net charge due to the following protonation equilibria:[17,18,57,58]

$$Al(OH)Al + H^+ = Al(OH_2)^+Al \quad (1)$$

$$\equiv SiOH = \equiv SiO^- + H^+ \quad (2)$$

The ζ potential *vs.* pH curve in water was markedly different from that measured in two cell culture media, F-12 and MEM, in which very similar curves were obtained. INT ζ potential is lower when passing from pure water to the two cell culture media, with the PZC shifting to lower pH values (pH = 4.2). Ions present in the two media may be adsorbed by INT, finally lowering the net charge, or, more likely the loss of positive charges is caused by adsorption of proteins from the serum present in the cell culture media.

Surface hydrophilicity and distribution of strong sites for water adsorption were investigated by means of adsorption microcalorimetry, following a technique established long time ago and previously employed for MWCNT[59] and amorphous silicas.[35,60] The adsorption isotherms of water vapor on INT pre-outgassed at 150°C are reported in Figure 4a while the energy of interaction as a function of coverage is reported in Figure 4b. The initial heat was extremely high, suggesting the presence of surface sites able to strongly interact with water. The whole energy as a function of coverage plot as well as uptakes revealed an extremely high hydrophilicity, opposite to MWCNT which are substantially hydrophobic.[59] The heat of interaction is even higher than what is usually found on silicas,[35,60] close to the behavior of alumina,[61] which is in substantial agreement with the model described in scheme 1 where the external layer is made up by aluminum octahedra.

Free radical generation

INT were tested for their potential in free radical release in the presence of either hydrogen peroxide (Fenton activity) or formiate ion (homolytic rupture of carbon-hydrogen bond), following a well established procedure. Two doses (7 and 70 mg) were tested. In all cases INT were fully inactive

(data not shown) as opposed to what has been previously reported to take placeon a large variety of toxic particles and fibers including asbestos.[6,62]

Imogolite nanotubes are less toxic than carbon nanotubes on macrophages

Effects of INT on cell viability, as assessed with the resazurin method, were compared with CNT (SWCNT and MWCNT), both known to exhibit marked cytotoxicity.[47,63] The effects of carbon nanotubes on the murine macrophage (RAW264.7 and MH-S) viability are shown in Figure 5. A clear cut dose-dependent toxicity was already evident for both SWCNT and MWCNT after 24h of incubation, with a significant decrease in viability detected in either cell line with the minimal nominal dose used (10 μg/cm^2), and a viability loss ≥ 80% detected at the maximal dose of 120 μg/cm^2. Under the same conditions, INT were completely ineffective up to 120 μg/cm^2 on MH-S cells, while only a modest 15% viability decrease was detected at 80 and 120 μg/cm^2 on RAW264.7 cells. Only for longer incubation periods INT showed significant effects on cell viability, up to a decrease of 35% at the maximal nominal dose (120 μg/cm^2) after 72h of treatment. Under the same conditions, the viability of the two macrophage lines was completely suppressed by either SWCNT or MWCNT.

Imogolite nanotubes do not induce markers of classical or alternative macrophage activation

The expression of activation markers in macrophages exposed to INT are shown in Figure 6. The gene for Arginase 1 (*Arg1*), a typical marker of alternative activation,[64-67] was not induced by INT in both RAW264.7 and MH-S macrophages, while both cell types exhibited a clear cut *Arg1* induction when incubated with IL-4, used as a positive control (Panels a and d). The expression of *Nos2* for the inducible isoform of nitric-oxide synthase, a marker of classical macrophage activation,[68-70] was also not stimulated by INT but several-fold increased by the positive control LPS (Panels b and e). The gene for Interleukin 6 (*Il6*), a pro-inflammatory cytokine not specifically

associated to either classical or alternative macrophage activation, was modestly induced by INT in RAW264.7 cells (Panel c), but not in MH-S macrophages, where a slight decrease was rather detected (Panel f).

The concentration of nitrites (as an indicator of NO production), determined in the extracellular medium of RAW264.7 cells incubated in the presence of INT, was not markedly different from that measured in control cells (Figure 7), consistent with the lack of *Nos2* induction observed under these conditions. On the contrary, nitrites were clearly accumulated in the extracellular medium of LPS-treated cultures. The nitrite concentration in the medium of LPS-treated cultures was comparable in the absence and in the presence of INT, indicating that imogolite did not affect the LPS-dependent *Nos2* induction

Imogolite nanotubes do not exert genotoxic effects

INT did not exert any DNA damage at all the doses and times investigated in RAW264.7 (Figure 8, Panel A), while a statistically significant increase of DNA damage was observed in A549 cells (Panel B) only at 80 μg/cm^2 after 4- and 24-h exposures. However, under the same conditions, while no cytotoxicity was reported for RAW264.7 cells (Table 2), a significant increase in cell death was observed for A549 cells (Table 3). Therefore, it cannot be completely ruled out that, DNA damage in epithelial cells was partially a consequence of cytotoxicity. CBMN-Cyt did not indicate any genotoxic effect after treatment with INT either in terms of MN frequency or of nucleoplasmic bridges in both the cell lines used (Fig. 9).

Imogolite nanotubes are internalized by macrophages

TEM analysis showed the presence of dense inclusions composed of highly packed fibrous material assigned to INT in the cytoplasm of exposed RAW264.7 cells (Figure 10). Due to its high density, the fibrous material was often partly dislocated during ultra-sectioning; however, it appeared to be

compartmentalized within membrane bound vacuoles (Figure. 10a). Such inclusions were never observed in the cytoplasm of control cells (Fig. 10b).

Imogolite nanotubes do not markedly alter the permeability of airway epithelial cell monolayers

A prolonged incubation with SWCNT or MWCNT progressively impairs the barrier properties of airway epithelial cells in a dose-dependent way.[47,63] To compare the effects of carbon nanotubes and INT on the airway epithelial barrier, confluent monolayers of Calu-3 cells were incubated with the three types of nanotubes at a nominal dose of 80 μg/cm^2 of monolayer. The trans-epithelial electrical resistance (TEER) was measured after seven days of treatment (Figure 11, Panel a). TEER was decreased by 50% in MWCNT-treated monolayers and by 40% in SWCNT-treated monolayers. On the contrary, INT did not alter TEER significantly, although the values were not significantly different from those measured in monolayers treated with SWCNT. Cell viability, evaluated with resazurin method (Panel b) in the same monolayers, was not significantly affected by any kind of nanotube.

DISCUSSION

Recently, the interest on aluminosilicates in biological systems has been renewed by the finding that they can form intracellularly at least in lower animals.[71] In these models, intracellular nanoparticles of aluminosilicates are considered non-toxic or even protective towards Al-mediated toxicity.[72] The biological effects of fibrous aluminosilicates are much less known and the possibility of toxic effects related to their high aspect-ratio has not been investigated in depth. The data reported in the present contribution clearly indicate that nanotubes of the aluminosilicate imogolite (INT) cause much milder cytotoxic effects than SWCNT and MWCNT on macrophages and airway epithelial cells.

In both the macrophage models adopted, RAW264.7 and MH-S cells, INT exerted a very modest, although significant, dose- and time-dependent cytotoxicity; after a 72h-exposure the IC_{50} was not reached at the maximal dose used of 120 $\mu g/cm^2$, and NOAEL was 10 $\mu g/cm^2$. Under the same conditions of exposure, both MWCNT and SWCNT caused a substantial loss of viability. Moreover, although INT were internalized in the macrophages, no evidence of genotoxic effects was obtained with the Comet and CBMN-Cyt assays in RAW264.7 cells. Lack of genotoxicity may be due to the fact that, as shown from the morphological evidence, INT are present as agglomerates in vacuoles and, hence, may be less able to reach intracellular sensitive targets, in analogy with what was described for MWCNT by Muller et al.[73] In addition, INT were not able to generate radical species in cell-free conditions. The absence of particle-derived free radical is not surprising since aluminium is a simple trivalent cation incapable of redox changes, and no impurities, e.g. transition metal ions, were detected on INT surface.

These data appear partially different from those reported for imogolite-like aluminogermanate nanofibers on cultured human fibroblasts,[25] where weak cytotoxicity but dose-dependent DNA damage and increased micronucleated cell frequency were detected even at very low concentrations of the “small” fibers (5-6 nm).[25] Weaker genotoxicity was observed with long fibers. Differences in

cell model, exposure times, fiber composition/length and absence of contaminants might account for different results exhibited by our study.

Besides reporting the low cytotoxic and genotoxic potential of INT, in the present study we also addressed the activating effects of INT on macrophages. Macrophages may react to nanomaterials eliciting several distinct activation pathways that determine tolerance to the material or ability to elicit inflammatory changes possibly followed by fibrotic alterations.[31,74-77] In both RAW264.7 and MH-S cells, INT do not induce *Arg1*, a typical marker of alternative macrophage activation[64-67], which underlies repair and fibrosis. Moreover, in the same models no induction of *Nos2*[68-70] was detected, indicating that INT do not promote the classical activation of macrophages, which is correlated to ROS production and tissue damage. The absence of *Nos2* induction is consistent with lack of nitrite accumulation in the medium, an indicator of NO production, and with the absence of marked cytotoxic effects. On the other hand, INT do not interfere with LPS-induced *Nos2* expression and nitrite accumulation. However, a significant induction of *Il6* was observed only in RAW264.7 cells but not in MH-S cells, suggesting that this finding is due more to specific features of the former cell line than to a response to INT shared by all macrophage cells. Thus, in conclusion, INT do not appear able to elicit definite changes typical of either classical or alternative macrophage activation, although it still may produce changes in gene expression depending on the particular cell type employed.

Airway epithelial cells are the first barrier that nanostructured materials have to cross to reach the lung interstitial tissues and to be transported thereafter to other districts of the organism. Interestingly, both fibrous silicates[78-80] and carbon nanotubes, either SWCNT or MWCNT,[47,63] have been reported to alter the barrier properties of airway Calu-3 epithelial cells *in vitro*. In contrast, after 7d of treatment, INT do not cause a significant increase of monolayer permeability on the same biological model, pointing to the substantial preservation of the epithelial cell barrier. These data also indicate that INT do not exert a significant cytotoxicity on the epithelial cells; indeed, if

only a minor portion of the epithelial cell population were damaged by INT, TEER would be expected to fall abruptly. However, since the TEER values recorded in monolayers treated with INT or SWCNT were not significantly different (Figure 11a), it is possible that also INT may damage the monolayer barrier at a longer incubation time. In conclusion, as far as epithelial barrier damage is concerned, the toxicity rank obtained is INT << SWCNT < MWCNT.

The mild effects of INT on all the cell models tested may be related both to the presence of bridged Al(OH)Al groups at the INT surface and to their high hydrophilicity. It is known since the beginning of the last century that aluminum ions are able to reduce the toxicity of crystalline silica.[81] The impregnation of quartz powders with an aluminum salt inhibits most adverse reactions to silica *in vivo* and decreases the generation of ROS and DNA damage caused by silica.[82,83] Mechanism of action of aluminum is poorly understood; however, it appears to affect the surface acidity reducing the zeta potential. The external layer of aluminum is also responsible for the positive surface charge of INT observed in large range of pH.

Moreover, the abundance of OH groups renders the structure very hydrophilic.[84] The presence of water strongly adsorbed at the surface is evidenced by the high heat of adsorption and confirmed by a previous study on the catalytic behavior of imogolite along with its thermal stability.[9] This study showed that the water inside nanotubes is completely desorbed only at 300 °C, whereas a temperature of 150 °C is sufficient to dehydrate amorphous silica. This strongly adsorbed water hinders molecular diffusion inside the narrow micropores.[9] Diffusion of molecules is also prevented because of the length of nanotubes, which can reach several μm. Moreover, silanols, which have been identified as the surface functionalities responsible for silica related cell membrane damage,[85] are all exposed in the inside of the INT and, hence, not available to cells.

In conclusion, while the morphology of INT suggests a potential toxicity, based on their high length-to-diameter ratio and expected durability, all the data reported point to mild, if any, toxic responses in a variety of cell models and tests upon exposure to this kind of material. The extreme

hydrophilicity and the presence of an external alumina layer in the absence of free radical release may contribute to the relative inertness of the material and support the feasibility of possible applications of INT in nanomedicine.

AUTHOR INFORMATION

Corresponding Authors

* B. F. Tel- +39 011 6707566 Fax +39 011 6707855 E-mail: bice.fubini@unito.it

* O.B. Tel. +39 0521 033783. Fax +39 0521 033742. E-mail: ovidio.bussolati@unipr.it

Funding

This work was supported by the Italian Ministry of University and Scientific-Technological Research (PRIN 2007498XRF, Study of the mechanisms responsible for cytotoxicity and genotoxicity of silica nanoparticles and nanometric fibrous silicates having strictly controlled size, structure and composition, national coordinator prof. Dario Ghigo). grants No. 2007498XRF_002 "Effects of silica nanoparticles and silicate nanofibers on lung-blood barrier cells" to O.B. and No. 2007498XRF_003 "Mechanisms responsible for cytotoxicity and genotoxicity of silica nanoparticles and nanometric fibrous silicates having strictly controlled size, structure and composition" to G.F.

Notes

The authors declare no competing financial interests. B.M.R., P.G., and B.B. equally contributed to this manuscript.

ACKNOWLEDGMENTS

The authors are thankful to Claudio Ghezzani for his technical assistance in image analysis. This work is part of the PhD thesis of P.G.

ABBREVIATIONS

BET, Brunauer-Emmett-Teller; CBMN, Cytokinesis-block Micronucleus Cytome; FBS, Fetal Bovine Serum; FE-SEM, Field Emission Scanning Electron Microscope; HARN, High-Aspect Ratio Nanomaterials; IEP, Iso-Electric Point; INT, imogolite nanotubes; LPS, lipopolysaccharide; MN, micronuclei; MWCNT, multi-walled carbon nanotubes; NL-DFT, Non Local Density Functional Theory; NOAEL, No Observed Adverse Effect Level; NPB, nucleoplasmic bridges; PSD, pore size distribution; SSA, Specific Surface Area; SWCNT, single-walled carbon nanotubes; TEER, Trans-Epithelial Electrical Resistance.

REFERENCES

(1) Kagan, V. E., Bayir, H., and Shvedova, A. A. (2005) Nanomedicine and nanotoxicology: two sides of the same coin. *Nanomedicine 1*, 313-316.

(2) Donaldson, K., Borm, P. J., Castranova, V., and Gulumian, M. (2009) The limits of testing particle-mediated oxidative stress in vitro in predicting diverse pathologies; relevance for testing of nanoparticles. *Part Fibre Toxicol 6*, 13.

(3) Xia, T., Li, N., and Nel, A. E. (2009) Potential health impact of nanoparticles. *Annu Rev Public Health 30*, 137-150.

(4) Oberdorster, G. (2010) Safety assessment for nanotechnology and nanomedicine: concepts of nanotoxicology. *J Intern Med 267*, 89-105.

(5) Donaldson, K., Murphy, F. A., Duffin, R., and Poland, C. A. (2010) Asbestos, carbon nanotubes and the pleural mesothelium: a review of the hypothesis regarding the role of long fibre retention in the parietal pleura, inflammation and mesothelioma. *Part Fibre Toxicol 7*, 5.

(6) Fubini, B., Fenoglio, I., Tomatis, M., and Turci, F. (2011) Effect of chemical composition and state of the surface on the toxic response to high aspect ratio nanomaterials. *Nanomedicine (Lond) 6*, 899-920.

(7) Donaldson, K., Murphy, F., Schinwald, A., Duffin, R., and Poland, C. A. (2011) Identifying the pulmonary hazard of high aspect ratio nanoparticles to enable their safety-by-design. *Nanomedicine (Lond) 6*, 143-156.

(8) Farmer, V. C. (1986) Sources and speciation of aluminium and silicon in natural waters. *Ciba Found Symp 121*, 4-23.

(9) Bonelli, B., Bottero, I., Ballarini, N., Passeri, S., Cavani, F., and Garrone, E. (2009) IR spectroscopic and catalytic characterization of the acidity of imogolite-based systems. *J Catal 264*, 15-30.

(10) Cradwick, P. D. G., Farmer, V. C., Russell, J. D., Masson, C. R., Wada, K., and Yoshinaga, N. (1972) Imogolite, a hydrated silicate of tubular nature. *Nature Physical Science 240*.

(11) Bonelli, B., Armandi, M., and Garrone, E. (2013) Surface properties of alumino-silicate single-walled nanotubes of the imogolite type. *Phys Chem Chem Phys*.

(12) Guimaraes, L., Pinto, Y. N., Lourenco, M. P., and Duarte, H. A. (2013) Imogolite-like nanotubes: structure, stability, electronic and mechanical properties of the phosphorous and arsenic derivatives. *Phys Chem Chem Phys 15*, 4303-4309.

(13) Gustafsson, J. P. (2001) The surface chemistry of imogolite. *Clay Clay Miner 49*, 73-80.

(14) Bottero, I., Bonelli, B., Ashbrook, S. E., Wright, P. A., Zhou, W. Z., Tagliabue, M., Armandi, M., and Garrone, E. (2011) Synthesis and characterization of hybrid organic/inorganic nanotubes of the imogolite type and their behaviour towards methane adsorption. *Physical Chemistry Chemical Physics 13*, 744-750.

(15) Pohl, P. I., Faulon, J. L., and Smith, D. M. (1996) Pore structure of imogolite computer models. *Langmuir 12*, 4463-4468.

(16) Ackerman, W. C., Smith, D. M., Huling, J. C., Kim, Y. W., Bailey, J. K., and Brinker, C. J. (1993) Gas Vapor Adsorption in Imogolite - a Microporous Tubular Aluminosilicate. *Langmuir 9*, 1051-1057.

(17) Clark, C. J., and McBride, M. B. (1984) Cation and anion retention by natural and synthetic allophane and imogolite. *Clay Clay Miner 32*, 291-299.

(18) Denaix, L., Lamy, I., and Bottero, J. Y. (1999) Structure and affinity towards Cd2+, Cu2+, Pb2+ of synthetic colloidal amorphous aluminosilicates and their precursors. *Colloid Surface A 158*, 315-325.

(19) Imamura, S., Kokubu, T., Yamashita, T., Okamoto, Y., Kajiwara, K., and Kanai, H. (1996) Shape-selective copper-loaded Imogolite catalyst. *J Catal 160*, 137-139.

(20) Levard, C., Rose, J., Masion, A., Doelsch, E., Borschneck, D., Olivi, L., Dominici, C., Grauby, O., Woicik, J. C., and Bottero, J. Y. (2008) Synthesis of large quantities of single-walled aluminogermanate nanotube. *J Am Chem Soc 130*, 5862-5863.

(21) Levard, C., Masion, A., Rose, J., Doelsch, E., Borschneck, D., Olivi, L., Chaurand, P., Dominici, C., Ziarelli, F., Thill, A., Maillet, P., and Bottero, J. Y. (2011) Synthesis of Ge-imogolite: influence of the hydrolysis ratio on the structure of the nanotubes. *Phys Chem Chem Phys 13*, 14516-14522.

(22) Levard, C., Masion, A., Rose, J., Doelsch, E., Borschneck, D., Dominici, C., Ziarelli, F., and Bottero, J. Y. (2009) Synthesis of imogolite fibers from decimolar concentration at low temperature and ambient pressure: a promising route for inexpensive nanotubes. *J Am Chem Soc 131*, 17080-17081.

(23) Maillet, P., Levard, C., Spalla, O., Masion, A., Rose, J., and Thill, A. (2011) Growth kinetic of single and double-walled aluminogermanate imogolite-like nanotubes: an experimental and modeling approach. *Phys Chem Chem Phys 13*, 2682-2689.

(24) Maillet, P., Levard, C., Larquet, E., Mariet, C., Spalla, O., Menguy, N., Masion, A., Doelsch, E., Rose, J., and Thill, A. (2010) Evidence of double-walled Al-Ge imogolite-like nanotubes. a cryo-TEM and SAXS investigation. *J Am Chem Soc 132*, 1208-1209.

(25) Liu, W., Chaurand, P., Di Giorgio, C., De Meo, M., Thill, A., Auffan, M., Masion, A., Borschneck, D., Chaspoul, F., Gallice, P., Botta, A., Bottero, J. Y., and Rose, J. (2012) Influence of the Length of Imogolite-Like Nanotubes on Their Cytotoxicity and Genotoxicity toward Human Dermal Cells. *Chemical Research in Toxicology 25*, 2513-2522.

(26) Ishikawa, K., Akasaka, T., Yawaka, Y., and Watari, F. (2010) High Functional Expression of Osteoblasts on Imogolite, Aluminosilicate Nanotubes. *Journal of Biomedical Nanotechnology 6*, 59-65.

(27) Farmer, V. C., Adams, M. J., Fraser, A. R., and Palmeri, F. (1983) Synthetic Imogolite: Properties, synthesis, and possible applications. *Clay Minerals 18*, 459-472.

(28) Landers, J., Gor, G. Y., and Neimark, A. V. (2013) Density functional theory methods for characterization of porous materials. *Colloid Surface A 437*, 3-32.

(29) Fubini, B., Mollo, L., and Giamello, E. (1995) Free radical generation at the solid/liquid interface in iron containing minerals. *Free Radic Res 23*, 593-614.

(30) Mbawuike, I. N., and Herscowitz, H. B. (1989) Mh-S, a Murine Alveolar Macrophage Cell-Line - Morphological, Cytochemical, and Functional-Characteristics. *J Leukocyte Biol 46*, 119-127.

(31) Xia, T., Kovochich, M., Brant, J., Hotze, M., Sempf, J., Oberley, T., Sioutas, C., Yeh, J. I., Wiesner, M. R., and Nel, A. E. (2006) Comparison of the abilities of ambient and manufactured nanoparticles to induce cellular toxicity according to an oxidative stress paradigm. *Nano Lett 6*, 1794-1807.

(32) Thibodeau, M., Giardina, C., and Hubbard, A. K. (2003) Silica-induced caspase activation in mouse alveolar macrophages is dependent upon mitochondrial integrity and aspartic proteolysis. *Toxicol Sci 76*, 91-101.

(33) Soto, K., Garza, K. M., and Murr, L. E. (2007) Cytotoxic effects of aggregated nanomaterials. *Acta Biomater 3*, 351-358.

(34) Scheel, J., Weimans, S., Thiemann, A., Heisler, E., and Hermann, M. (2009) Exposure of the murine RAW 264.7 macrophage cell line to hydroxyapatite dispersions of various composition and morphology: Assessment of cytotoxicity, activation and stress response. *Toxicol in Vitro 23*, 531-538.

(35) Ghiazza, M., Polimeni, M., Fenoglio, I., Gazzano, E., Ghigo, D., and Fubini, B. (2010) Does Vitreous Silica Contradict the Toxicity of the Crystalline Silica Paradigm? *Chemical Research in Toxicology 23*, 620-629.

(36) Gonzalez, L., Thomassen, L. C., Plas, G., Rabolli, V., Napierska, D., Decordier, I., Roelants, M., Hoet, P. H., Kirschhock, C. E., Martens, J. A., Lison, D., and Kirsch-Volders, M. (2010)

Exploring the aneugenic and clastogenic potential in the nanosize range: A549 human lung carcinoma cells and amorphous monodisperse silica nanoparticles as models. *Nanotoxicology 4*, 382-395.

(37) Guidi, P., Nigro, M., Bernardeschi, M., Scarcelli, V., Lucchesi, P., Onida, B., Mortera, R., and Frenzilli, G. (2013) Genotoxicity of amorphous silica particles with different structure and dimension in human and murine cell lines. *Mutagenesis 28*, 171-180.

(38) Finkbeiner, W. E., Carrier, S. D., and Teresi, C. E. (1993) Reverse Transcription-Polymerase Chain-Reaction (Rt-Pcr) Phenotypic Analysis of Cell-Cultures of Human Tracheal Epithelium, Tracheobronchial Glands, and Lung Carcinomas. *Am J Resp Cell Mol 9*, 547-556.

(39) Grainger, C. I., Greenwell, L. L., Martin, G. P., and Forbes, B. (2009) The permeability of large molecular weight solutes following particle delivery to air-interfaced cells that model the respiratory mucosa. *Eur J Pharm Biopharm 71*, 318-324.

(40) Togami, K., Chono, S., Seki, T., and Morimoto, K. (2009) Distribution Characteristics of Telithromycin, a Novel Ketolide Antimicrobial Agent Applied for Treatment of Respiratory Infection, in Lung Epithelial Lining Fluid and Alveolar Macrophages. *Drug Metab Pharmacok 24*, 411-417.

(41) Slutter, B., Bal, S. M., Que, I., Kaijzel, E., Lowik, C., Bouwstra, J., and Jiskoot, W. (2010) Antigen-Adjuvant Nanoconjugates for Nasal Vaccination: An Improvement over the Use of Nanoparticles? *Mol Pharmaceut 7*, 2207-2215.

(42) Brillault, J., De Castro, W. V., and Couet, W. (2010) Relative contributions of active mediated transport and passive diffusion of fluoroquinolones with various lipophilicities in a Calu-3 lung epithelial cell model. *Antimicrob Agents Chemother 54*, 543-545.

(43) Bharatwaj, B., Wu, L. B., Whittum-Hudson, J. A., and da Rocha, S. R. P. (2010) The potential for the noninvasive delivery of polymeric nanocarriers using propellant-based inhalers in the treatment of Chlamydial respiratory infections. *Biomaterials 31*, 7376-7385.

(44) Bur, M., Huwer, H., Muys, L., and Lehr, C. M. (2010) Drug Transport Across Pulmonary Epithelial Cell Monolayers: Effects of Particle Size, Apical Liquid Volume, and Deposition Technique. *J Aerosol Med Pulm D 23*, 119-127.

(45) Burgess, B. L., Cavigiolio, G., Fannucchi, M. V., Illek, B., Forte, T. M., and Oda, M. N. (2010) A phospholipid-apolipoprotein A-I nanoparticle containing amphotericin B as a drug delivery platform with cell membrane protective properties. *Int J Pharmaceut 399*, 148-155.

(46) O'Brien, J., Wilson, I., Orton, T., and Pognan, F. (2000) Investigation of the Alamar Blue (resazurin) fluorescent dye for the assessment of mammalian cell cytotoxicity. *Eur J Biochem 267*, 5421-5426.

(47) Rotoli, B. M., Bussolati, O., Bianchi, M. G., Barilli, A., Balasubramanian, C., Bellucci, S., and Bergamaschi, E. (2008) Non-functionalized multi-walled carbon nanotubes alter the paracellular permeability of human airway epithelial cells. *Toxicol Lett 178*, 95-102.

(48) Bianchi, M. G., Gazzola, G. C., Tognazzi, L., and Bussolati, O. (2008) C6 glioma cells differentiated by retinoic acid overexpress the glutamate transporter excitatory amino acid carrier 1 (eaac1). *Neuroscience 151*, 1042-1052.

(49) Visigalli, R., Barilli, A., Bussolati, O., Sala, R., Gazzola, G. C., Parolari, A., Tremoli, E., Simon, A., Closs, E. I., and Dall'Asta, V. (2007) Rapamycin stimulates arginine influx through CAT2 transporters in human endothelial cells. *Biochim Biophys Acta 1768*, 1479-1487.

(50) Guidi, P., Nigro, M., Bernardeschi, M., Scarcelli, V., Lucchesi, P., Onida, B., Mortera, R., and Frenzilli, G. (2013) Genotoxicity of amorphous silica particles with different structure and dimension in human and murine cell lines. *Mutagenesis 28*, 171-180.

(51) Singh, N. P., McCoy, M. T., Tice, R. R., and Schneider, E. L. (1988) A simple technique for quantitation of low levels of DNA damage in individual cells. *Exp Cell Res 175*, 184-191

(52) Fenech, M., Chang, W. P., Kirsch-Volders, M., Holland, N., Bonassi, S., and Zeiger, E. (2003) HUMN project: detailed description of the scoring criteria for the cytokinesis-block micronucleus assay using isolated human lymphocyte cultures. *Mutat Res 534*, 65-75.

(53) Fenech, M. (2007) Cytokinesis-block micronucleus cytome assay. *Nat Protoc 2*, 1084-1104.

(54) Salem, L. B., Bosquillon, C., Dailey, L. A., Delattre, L., Martin, G. P., Evrard, B., and Forbes, B. (2009) Sparing methylation of beta-cyclodextrin mitigates cytotoxicity and permeability induction in respiratory epithelial cell layers in vitro. *J Control Release 136*, 110-116.

(55) Mollenhauer, H. H. (1964) Plastic Embedding Mixtures for Use in Electron Microscopy. *Stain Technol 39*, 111-114.

(56) Singh, B. P., Menchavez, R., Takai, C., Fuji, M., and Takahashi, M. (2005) Stability of dispersions of colloidal alumina particles in aqueous suspensions. *J Colloid Interf Sci 291*, 181-186.

(57) Arai, Y., McBeath, M., Bargar, J. R., Joye, J., and Davis, J. A. (2006) Uranyl adsorption and surface speciation at the imogolite-water interface: Self-consistent spectroscopic and surface complexation models. *Geochim Cosmochim Ac 70*, 2492-2509.

(58) Park, S., Lee, Y., Kim, B., Lee, J., Jeong, Y., Noh, J., Takahara, A., and Sohn, D. (2007) Two-dimensional alignment of imogolite on a solid surface. *Chem Commun (Camb)*, 2917-2919.

(59) Fenoglio, I., Greco, G., Tomatis, M., Muller, J., Raymundo-Pinero, E., Beguin, F., Fonseca, A., Nagy, J. B., Lison, D., and Fubini, B. (2008) Structural defects play a major role in the acute lung toxicity of multiwall carbon nanotubes: physicochemical aspects. *Chem Res Toxicol 21*, 1690-1697.

(60) Gazzano, E., Ghiazza, M., Polimeni, M., Bolis, V., Fenoglio, I., Attanasio, A., Mazzucco, G., Fubini, B., and Ghigo, D. (2012) Physicochemical determinants in the cellular responses to nanostructured amorphous silicas. *Toxicol Sci 128*, 158-170.

(61) Fubini, B., Della Gatta, G., and Venturello, G. (1978) Energetics of adsorption in the alumina water system. Microcalorimetric study on the influence of adsorption temperature on surface processes. *J. Colloid and Interface Science 64*, 470-479.

(62) Fubini, B., and Hubbard, A. (2003) Reactive oxygen species (ROS) and reactive nitrogen species (RNS) generation by silica in inflammation and fibrosis. *Free Radic Biol Med 34*, 1507-1516.

(63) Rotoli, B. M., Bussolati, O., Barilli, A., Zanello, P. P., Bianchi, M. G., Magrini, A., Pietroiusti, A., Bergamaschi, A., and Bergamaschi, E. (2009) Airway barrier dysfunction induced by exposure to carbon nanotubes in vitro: which role for fiber length? *Hum Exp Toxicol 28*, 361-368.

(64) Louis, C. A., Mody, V., Henry, W. L., Reichner, J. S., and Albina, J. E. (1999) Regulation of arginase isoforms I and II by IL-4 in cultured murine peritoneal macrophages. *Am J Physiol-Reg I 276*, R237-R242.

(65) Morris, S. M., Kepka-Lenhart, D., and Chen, L. C. (1998) Differential regulation of arginases and inducible nitric oxide synthase in murine macrophage cells. *Am J Physiol-Endoc M 275*, E740-E747.

(66) Stempin, C., Giordanengo, L., Gea, S., and Cerban, F. (2002) Alternative activation and increase of Trypanosoma cruzi survival in murine macrophages stimulated by cruzipain, a parasite antigen. *J Leukocyte Biol 72*, 727-734.

(67) Raes, G., Van den Bergh, R., De Baetselier, P., Ghassabeh, G. H., Scotton, C., Locati, M., Mantovani, A., and Sozzani, S. (2005) Arginase-1 and Ym1 are markers for murine, but not human, alternatively activated myeloid cells. *J Immunol 174*, 6561; author reply 6561-6562.

(68) Yamashita, M., Niki, H., Yamada, M., Mue, S., and Ohuchi, K. (1997) Induction of nitric oxide synthase by lipopolysaccharide and its inhibition by auranofin in RAW 264.7 cells. *Eur J Pharmacol 338*, 151-158.

(69) Munder, M., Eichmann, K., Moran, J. M., Centeno, F., Soler, G., and Modolell, M. (1999) Th1/Th2-regulated expression of arginase isoforms in murine macrophages and dendritic cells. *J Immunol 163*, 3771-3777.

(70) Chakravortty, D., Kato, Y., Sugiyama, T., Koide, N., Mu, M. M., Yoshida, T., and Yokochi, T. (2001) The inhibitory action of sodium arsenite on lipopolysaccharide-induced nitric oxide production in RAW 267.4 macrophage cells: a role of Raf-1 in lipopolysaccharide signaling. *J Immunol 166*, 2011-2017.

(71) White, K. N., Ejim, A. I., Walton, R. C., Brown, A. P., Jugdaohsingh, R., Powell, J. J., and McCrohan, C. R. (2008) Avoidance of aluminum toxicity in freshwater snails involves intracellular silicon-aluminum biointeraction. *Environ Sci Technol 42*, 2189-2194.

(72) Jugdaohsingh, R., Brown, A., Dietzel, M., and Powell, J. J. (2013) High-aluminum-affinity silica is a nanoparticle that seeds secondary aluminosilicate formation. *PLoS One 8*, e84397.

(73) Muller, J., Huaux, F., Moreau, N., Misson, P., Heilier, J. F., Delos, M., Arras, M., Fonseca, A., Nagy, J. B., and Lison, D. (2005) Respiratory toxicity of multi-wall carbon nanotubes. *Toxicol Appl Pharmacol 207*, 221-231.

(74) Bergamaschi, E., Bussolati, O., Magrini, A., Bottini, M., Migliore, L., Bellucci, S., Iavicoli, I., and Bergamaschi, A. (2006) Nanomaterials and lung toxicity: interactions with airways cells and relevance for occupational health risk assessment. *Int J Immunopathol Pharmacol 19*, 3-10.

(75) Sanchez, V. C., Pietruska, J. R., Miselis, N. R., Hurt, R. H., and Kane, A. B. (2009) Biopersistence and potential adverse health impacts of fibrous nanomaterials: what have we learned from asbestos? *Wires Nanomed Nanobi 1*, 511-529.

(76) Shvedova, A. A., and Kagan, V. E. (2010) The role of nanotoxicology in realizing the 'helping without harm' paradigm of nanomedicine: lessons from studies of pulmonary effects of single-walled carbon nanotubes. *Journal of Internal Medicine 267*, 106-118.

(77) Nagai, H., and Toyokuni, S. (2010) Biopersistent fiber-induced inflammation and carcinogenesis: Lessons learned from asbestos toward safety of fibrous nanomaterials. *Arch Biochem Biophys 502*, 1-7.

(78) Peterson, M. W., Walter, M. E., and Gross, T. J. (1993) Asbestos Directly Increases Lung Epithelial Permeability. *Am J Physiol 265*, L308-L317.

(79) Gardner, S. Y., Brody, A. R., Mangum, J. B., and Everitt, J. I. (1997) Chrysotile asbestos and H2O2 increase permeability of alveolar epithelium. *Exp Lung Res 23*, 1-16.

(80) Peterson, M. W., and Kirschbaum, J. (1998) Asbestos-induced lung epithelial permeability: Potential role of nonoxidant pathways. *Am J Physiol-Lung C 275*, L262-L268.

(81) Fubini, B., Health effects of silica. In *The surface properties of silicas*, J.P., L., Ed. J. Wiley and Sons: 1998; pp 415-464.

(82) Duffin, R., Gilmour, P. S., Schins, R. P. F., Clouter, A., Guy, K., Brown, D. M., MacNee, W., Borm, P. J., Donaldson, K., and Stone, V. (2001) Aluminium lactate treatment of DQ12 quartz inhibits its ability to cause inflammation, chemokine expression, and nuclear factor-kappa B activation. *Toxicol Appl Pharm 176*, 10-17.

(83) Knaapen, A. M., Albrecht, C., Becker, A., Hohr, D., Winzer, A., Haenen, G. R., Borm, P. J. A., and Schins, R. P. F. (2002) DNA damage in lung epithelial cells isolated from rats exposed to quartz: role of surface reactivity and neutrophilic inflammation. *Carcinogenesis 23*, 1111-1120.

(84) Creton, B., Bougeard, D., Smirnov, K. S., Guilment, J., and Poncelet, O. (2008) Molecular dynamics study of hydrated imogolite. 2. Structure and dynamics of confined water. *Phys Chem Chem Phys 10*, 4879-4888.

(85) Slowing, I. I., Wu, C. W., Vivero-Escoto, J. L., and Lin, V. S. Y. (2009) Mesoporous Silica Nanoparticles for Reducing Hemolytic Activity Towards Mammalian Red Blood Cells. *Small 5*, 57-62.

Table 1

Primers used for RT-PCR studies

Gene	Forward	Reverse
Arg1	5' CAG AAG AAT GGA AGA GTC AG 3'	5' GGA GTG TTG ATG TCA GTG TG 3'
Nos2	5' GTT CTC AGC CCA ACA ATA CAA GA 3'	5' GTG GAC GGG TCG ATG TCA C 3'
Il6	5' TAG TCC TTC CTA CCC CAA TTT CC 3'	5' TTG GTC CTT AGC CAC TCC TTC 3'
Gapdh	5' TGT TCC TAC CCC CAA TGT GT 3'	5' GGT CCT CAG TGT AGC CCA AG 3'

Table 2

Viability of RAW264.7 cells

Cell viability, %							
Imogolite ($\mu g/cm^2$)	**0**	**C+**	**5**	**10**	**20**	**40**	**80**
4h	100±0.0	83±26.1	95±5.7	96±7,2	94±3.6	84±16.8	88±8.5
24h	95± 8.4	90±8.6	100±0.0	95±10.0	100±0.2	99±0.9	96±4.5

Values are means ± SD. C+ = methylmethanesulfonate 0.5mM

Table 3

Viability of A549 cells

Cell viability, %							
Imogolite ($\mu g/cm^2$)	**0**	**C+**	**5**	**10**	**20**	**40**	**80**
4h	97±3.2	98±2.4	95±5.6	94±1.9	93±1.3	93±3.5	91±4.8*
24h	95±5.5	91±0.1	94±0.2	89±4.8	92±4.1	86±5.0*	88±6.8*

Values are means ± SD. C+ = methylmethanesulfonate 0.5mM. * $p < 0.05$ vs. untreated cells.

FIGURE LEGENDS

Scheme 1. Cross-section of an imogolite nanotube showing its chemical composition. The inner diameter is about 1.0 nm.

Scheme 2. Bundles of INT with (A) intra-tube pores; (B) inter-tubes pores; and (C) slit mesopores among bundles.

Figure 1. Selected FE-SEM micrographs of INT (a), SWCNT (b) and MWCNT (c).

Figure 2. a) N_2 isotherm at –196 °C on INT outgassed at 300 °C: black symbols adsorption branch; white symbols: desorption branch. b) PSD of INT outgassed at 300 °C as obtained according to NL-DFT method by applying a nitrogen-silica kernel to the adsorption branch of the isotherm.

Figure 3. ζ- potential curves of INT in water (black circles), F-12 medium (triangles) and MEM medium (white squares). Media were supplemented with 10% FBS.

Figure 4. Adsorption of H_2O_{vap} at T = 30°C on imogolite nanotubes outgassed 2 h at 150°C. (a) amount of water adsorbed as a function of the equilibrium pressure (n_{ads} vs. p_{H2O}). (b) Differential heat of adsorption as a function of the surface coverage (qdiff vs. n_{ads}). Full symbols, total adsorption (Ads I); empty symbols, reversible adsorption (Ads II).

Figure 5. INT and SWCNT effects on macrophage viability. Subconfluent cultures of RAW264.7 and MH-S murine macrophages, grown on 96-well dishes, were exposed for the indicated times to nominal doses of INT, SWCNT and MWCNT ranging from 0 to 120 μg/cm^2, corresponding to 192

μg/ml. At the selected times, viability was assessed with the resazurin method . Data are means of 5 independent determinations with SD in a representative experiment performed four times with comparable results. * p<0.05, **p< 0.01, *** p <0.001 *vs.* control, untreated cultures.

Figure 6. INT effects on gene expression in murine macrophages. RAW264.7 (Panels a, b, c) or MH-S cells (Panels d, e, f) were incubated for 72h in the presence of INT (120 μg/cm^2, 72h), IL-4 (10 ng/ml, 24h), or LPS (0.1 μg/ml, 18h), as indicated. At the end of the treatment, mRNA was extracted and the abundance of the mRNAs of *Arg1* (Panels a, d), *Nos2* (Panels b, e), and *Il6* (Panels c, f) was determined and expressed *vs.* the abundance of *Gapdh* mRNA. Data represent means of three independent determinations, each performed in duplicate (n = 3), with SD shown. *p < 0.05, ** p < 0.01 *vs.* control.

Figure 7. INT effects on nitrite concentration in the growth medium of murine macrophages. RAW264.7 cells were incubated for 72h in the presence of INT (120 μg/cm^2, 72h) or LPS (0.1 μg/ml, 18h), or both, as indicated. The concentration of nitrites in the extracellular medium was determined at the end of the treatment. Data represent means of six independent determinations with SD obtained in a representative experiment, performed two times with comparable results. *** p < 0.001 *vs.* control.

Figure 8. DNA damage (% DNA in tail) in RAW264.7 (a) and A549 (b) cell lines exposed to different INT doses for 4 and 24 h. 0.5 mM methylmethanesulfonate (MMS) was used as positive control. * indicates significant difference (Multiple Range Test) with the other experimental points (p < 0.05).

Figure 9. Frequency of micronuclei and nucleoplasmic bridges (NPB) in RAW264.7 (a) and A549 (b) cells after exposure to different INT doses. Mitomycin C was used as positive control. * indicates significant difference (Multiple Range Test) with the other experimental points ($p < 0.05$). N.D.: not enough cells to perform cytogenetic analyses.

Figure 10. Transmission electron micrographs of RAW264.7 cells. Cells were incubated in the absence or in the presence of 80 μg/cm^2 INT for 24 hours. a: Exposed cell showing a densely packed imogolite inclusion (arrow). b: Control cell devoid of dense inclusions. N= nucleus; scale bars = 1 μm for a; 2 μm for b.

Figure 11. Differential effects of INT, SWCNT and MWCNT on the trans-epithelial electrical resistance (TEER) and viability of Calu-3 monolayers. Calu-3 cells were cultured for 10 days on 0.4 μm membrane filters. At the end of this period, INT, SWCNT, or MWCNT, all at 80 μg/cm^2, were added to the apical chamber of the culture system. TEER (Panel a) and viability (Panel b) were determined after 7 days. Empty bar, control monolayers maintained in the absence of nanomaterials. The figure shows a representative experiment performed three times with comparable results. Data are means ± SD (n = 4). $^{**}p < 0.01$ *vs.* control, untreated cultures; $ $p < 0.05$ vs. MWCNT-treated monolayers; ns, not significant.

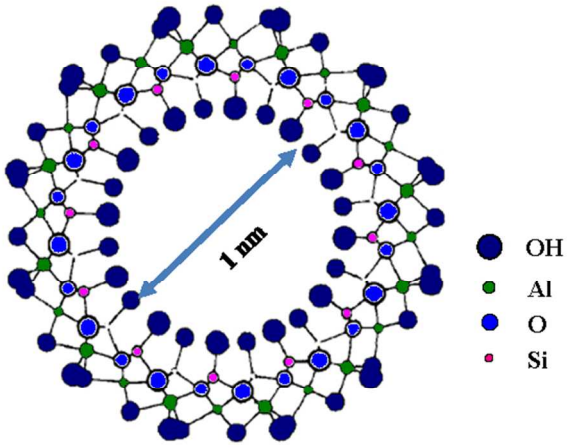

Scheme 1. Cross-section of an imogolite nanotube showing its chemical composition. The inner diameter is about 1.0 nm.
254x190mm (96 x 96 DPI)

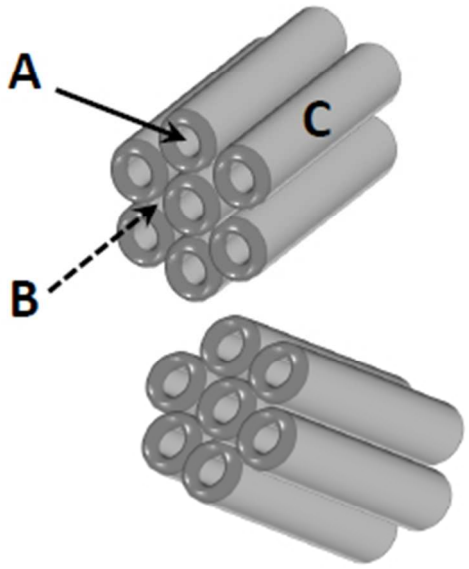

Scheme 2. Bundles of INT with (A) nanotubes inherent pores; (B) inter-tubes pores; and (C) slit mesopores among bundles.

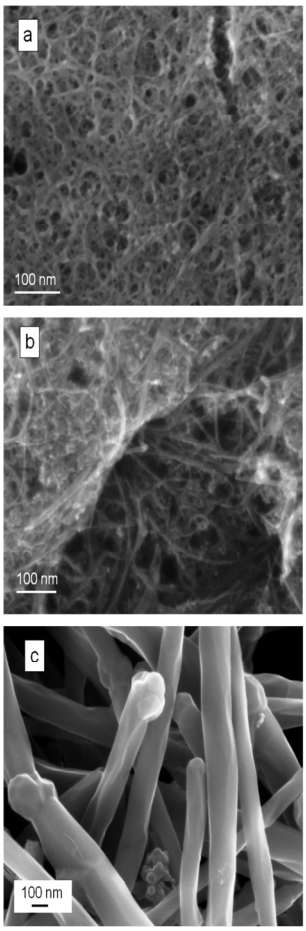

Figure 1. Selected FE-SEM micrographs of INT (a), SWCNT (b) and MWCNT (c).
190x254mm (220 x 220 DPI)

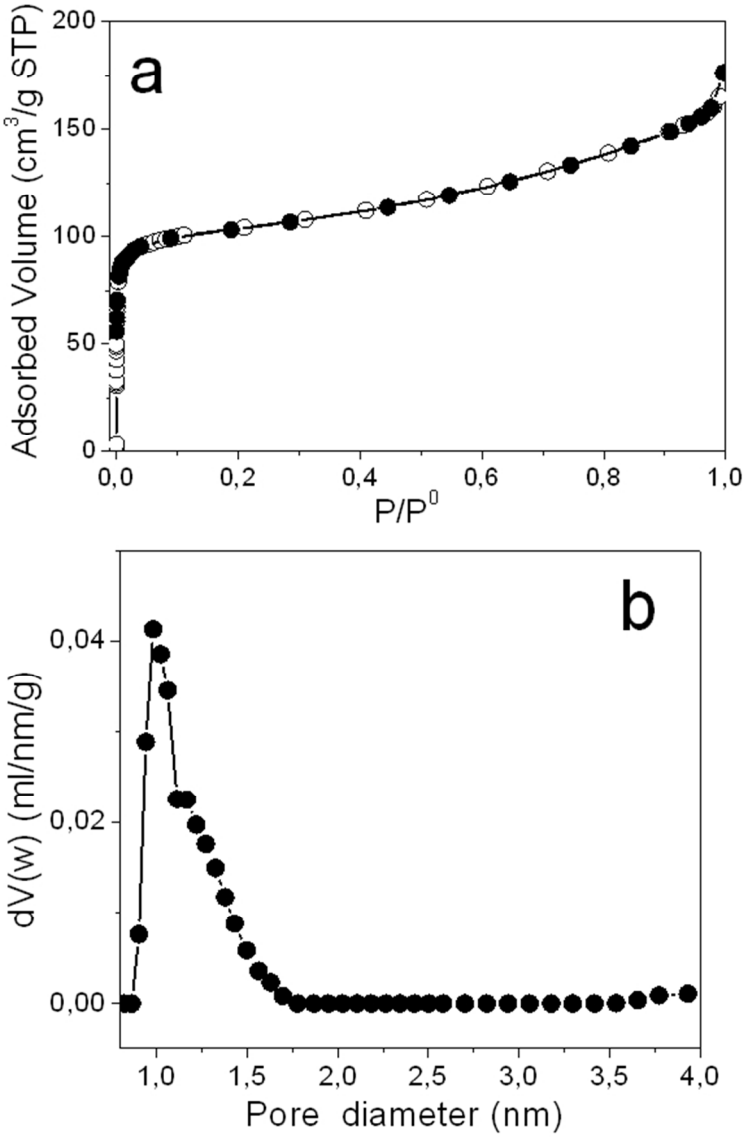

Figure 2. a) N2 isotherm at –196 °C on INT outgassed at 300 °C: black symbols adsorption branch; white symbols: desorption branch. b) PSD of INT outgassed at 300 °C as obtained according to NL-DFT method by applying a nitrogen-silica kernel to the adsorption branch of the isotherm.

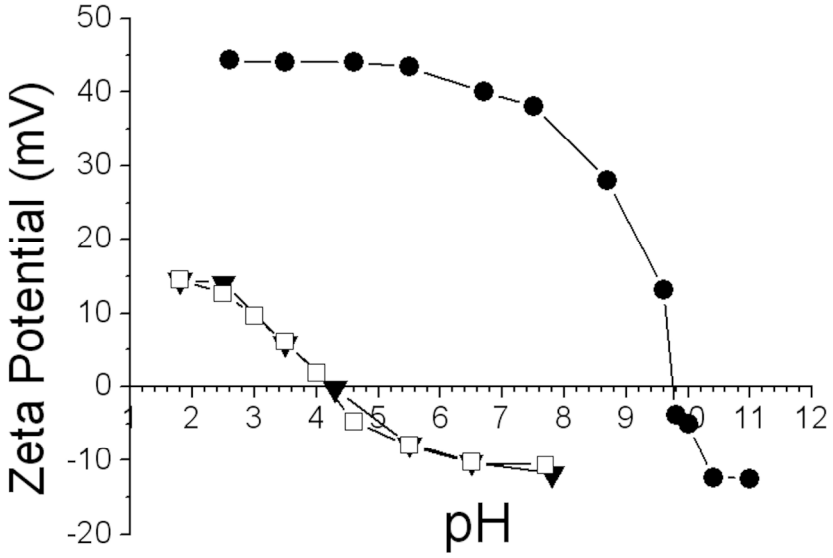

Figure 3. ζ potential curves of INT in water (black circles), in F-12 (triangles) and MEM (white squares).

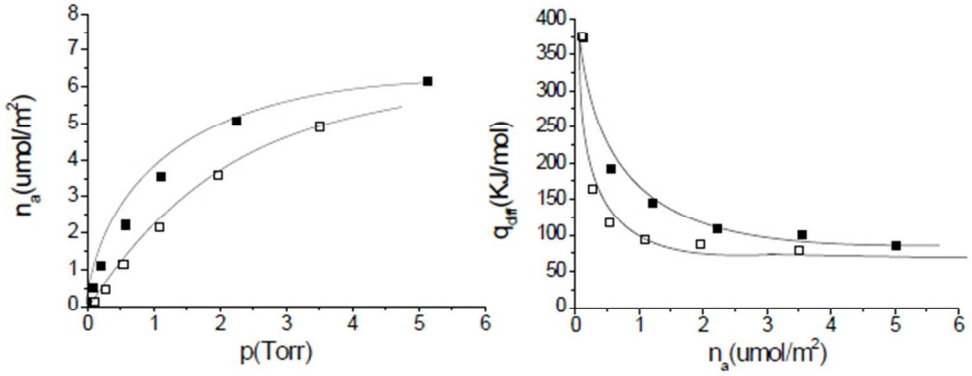

Figure 4. Adsorption of H2Ovap at T = 30°C on imogolite nanotubes outgassed 2 h at 150°C. (a) amount of water adsorbed as a function of the equilibrium pressure (nads vs. pH2O). (b) Differential heat of adsorption as
a function of the surface coverage (qdiff vs. nads). Full symbols, total adsorption (Ads I); empty symbols, reversible adsorption (Ads II).

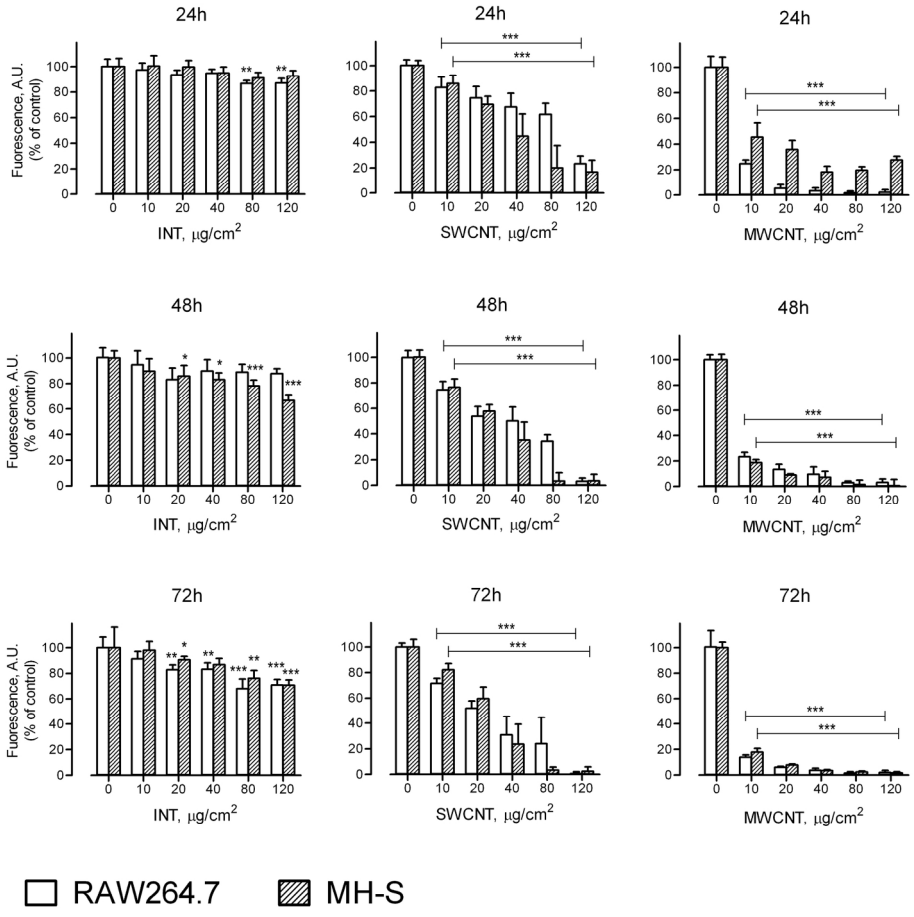

Figure 5. INT and SWCNT effects on macrophage viability. Subconfluent cultures of RAW264.7 and MH-S murine macrophages, grown on 96-well dishes, were exposed for the indicated times to nominal doses of INT, SWCNT and MWCNT ranging from 0 to 120 μg/cm^2, corresponding to 192 μg/ml. At the selected times, viability was assessed with the resazurin method . Data are means of 5 independent determinations with SD in a representative experiment performed four times with comparable results. * $p<0.05$, **$p< 0.01$, *** $p <0.001$ vs. control, untreated cultures.
175x168mm (300 x 300 DPI)

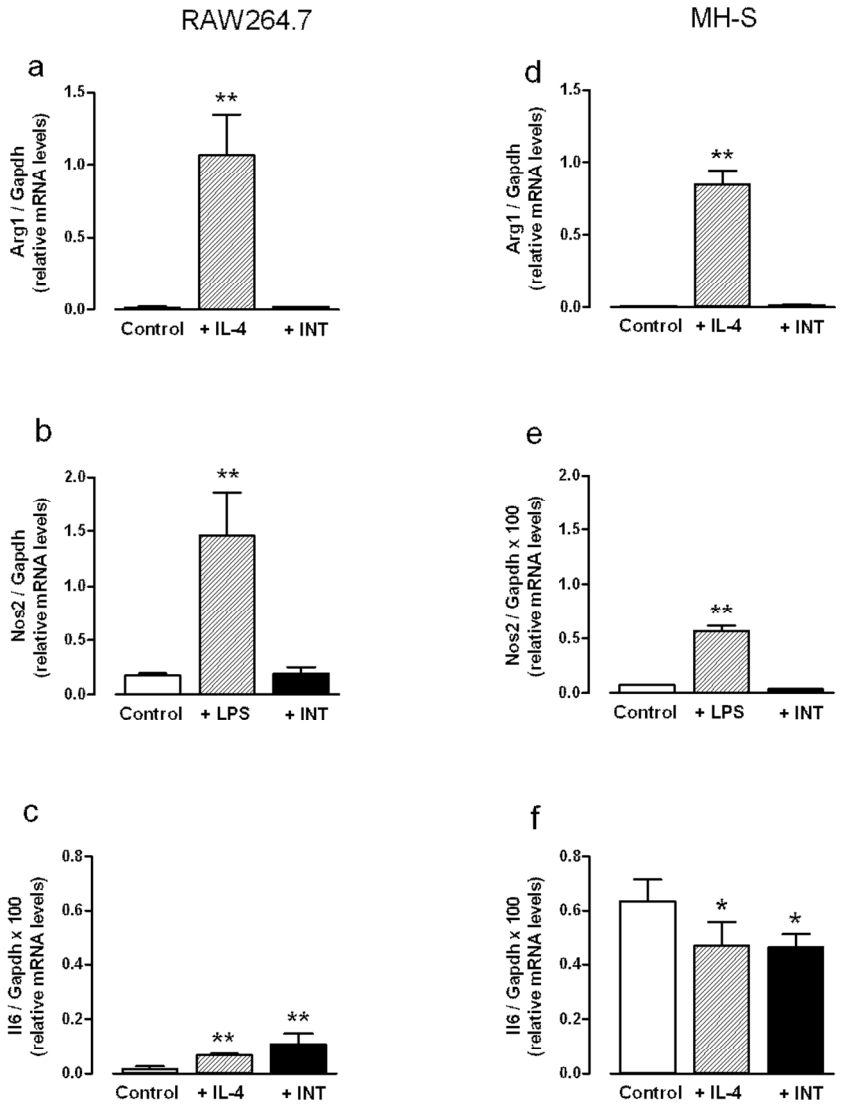

Figure 6. INT effects on gene expression in murine macrophages. RAW264.7 (Panels a, b, c) or MH-S cells (Panels d, e, f) were incubated for 72h in the presence of INT (120 μg/cm^2, 72h), IL-4 (10 ng/ml, 24h), or LPS (0.1 μg/ml, 18h), as indicated. At the end of the treatment, mRNA was extracted and the abundance of the mRNAs of *Arg1* (Panels a, d), *Nos2* (Panels b, e), and *Il6* (Panels c, f) was determined and expressed vs. the abundance of *Gapdh* mRNA. Data represent means of three independent determinations, each performed in replicate, with SD shown. *p < 0.05, ** p < 0.01 vs. control.
98x129mm (300 x 300 DPI)

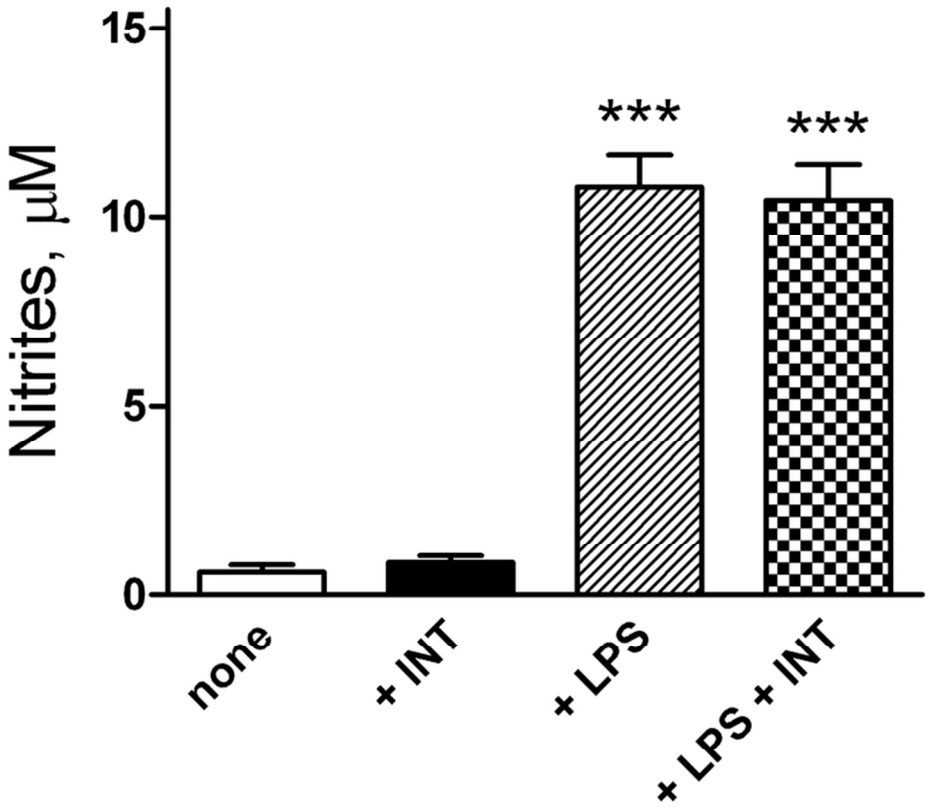

Figure 7. INT effects on nitrite concentration in the growth medium of murine macrophages. RAW264.7 cells were incubated for 72h in the presence of INT (120 μg/cm^2, 72h) or LPS (0.1 μg/ml, 18h), or both, as indicated. The concentration of nitrites in the extracellular medium was determined at the end of the treatment. Data represent means of six independent determinations with SD obtained in a representative experiment, performed two times with comparable results. *** $p < 0.001$ vs. control.
73x67mm (300 x 300 DPI)

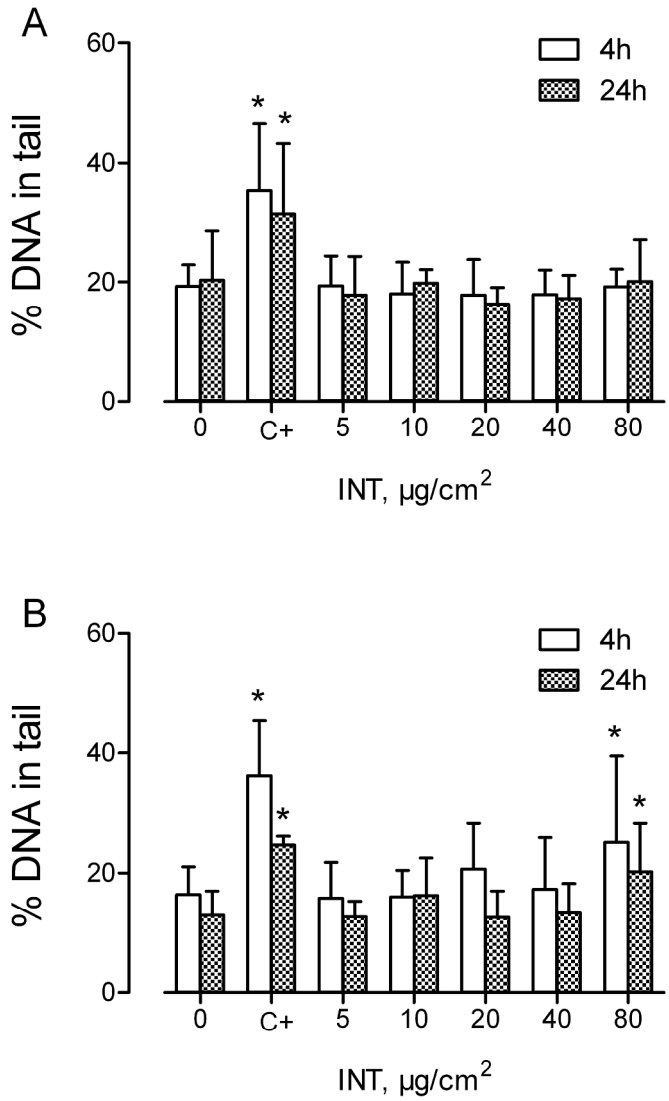

Figure 8. DNA damage (% DNA in tail) in RAW264.7 (a) and A549 (b) cell lines exposed to different INT doses for 4 and 24 h. 0.5 mM methylmethanesulfonate (MMS) was used as positive control. * indicates significant difference (Multiple Range Test) with the other experimental points ($p < 0.05$).
115x167mm (600 x 600 DPI)

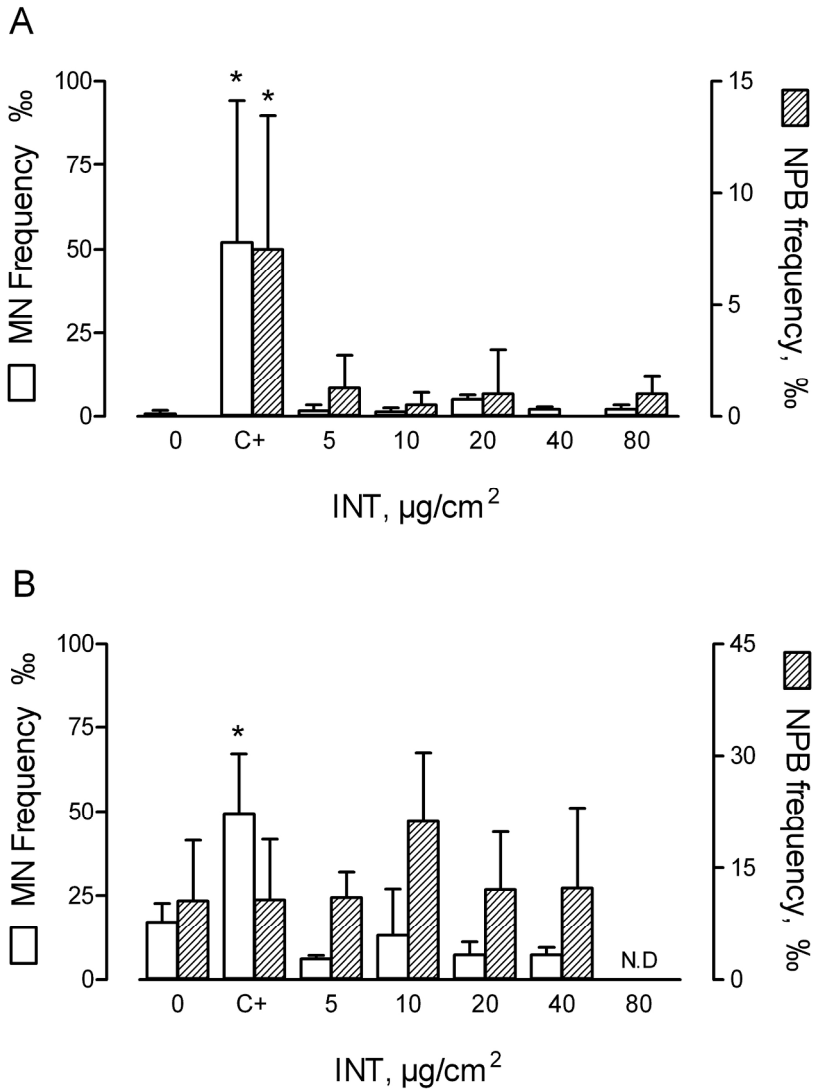

Figure 9. Frequency of micronuclei and nucleoplasmic bridges (NPB) in RAW264.7 (a) and A549 (b) cells after exposure to different INT doses. Mitomycin C was used as positive control. * indicates significant difference (Multiple Range Test) with the other experimental points ($p < 0.05$). N.D. not enough cells to perform cytogenetic analyses.
102x131mm (600 x 600 DPI)

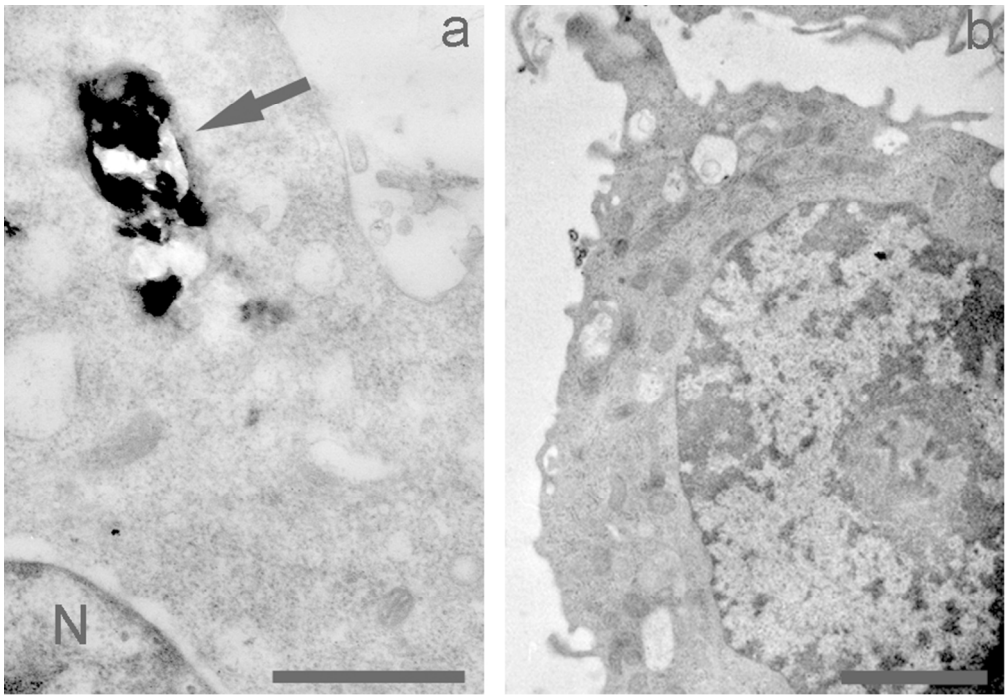

Figure 10. Transmission electron micrographs of RAW 264.7 cells. Cells were incubated in the absence or in the presence of 80 µg/cm2 INT for 24 hours. a. Exposed cell showing a densely packed imogolite inclusion (arrow). b. Control cell devoid of dense inclusions. N= nucleus; scale bars = 1 µm for a; 2 µm for b.
77x53mm (300 x 300 DPI)

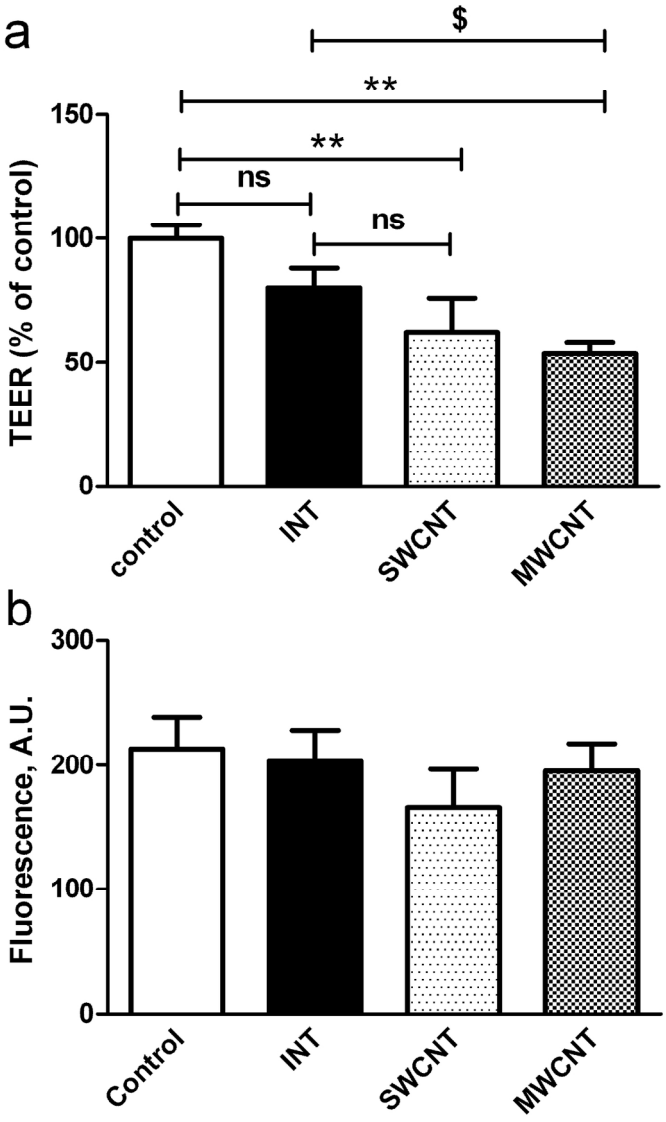

Figure 11. Differential effects of INT, SWCNT and MWCNT on the trans-epithelial electrical resistance (TEER) and viability of Calu-3 monolayers. Calu-3 cells were cultured for 10 days on 0.4 µm membrane filters. At the end of this period, INT, SWCNT, or MWCNT, all at 80 µg/cm^2, were added to the apical chamber of the culture system. TEER (Panel A) and viability (Panel B) were determined after 7 days. Empty bar, control monolayers maintained in the absence of nanomaterials. The figure shows a representative experiment performed three times with comparable results. Data are means ± SD (n = 4). **p < 0.01 vs. control, untreated cultures; $ p < 0.05 vs. MWCNT-treated monolayers; ns, not significant.
129x210mm (300 x 300 DPI)